

The Horizontal Branch in the UV colour Magnitude Diagrams. II. The case of M3, M13 and M79.

E. Dalessandro,¹ M. Salaris,² F.R. Ferraro,¹ A. Mucciarelli,¹ S. Cassisi,³

¹*Dipartimento di Fisica e Astronomia, Università degli Studi di Bologna, viale Berti Pichat 6/2, I-40127 Bologna, Italy*

²*Astrophysics Research Institute, Liverpool John Moores University, Twelve Quays House, Egerton Wharf, Birkenhead CH41 1LD, UK*

³*INAF - Osservatorio Astronomico di Collurania, via Mentore Maggini, 64100 Teramo, Italy*

18 December, 2012

ABSTRACT

We present a detailed comparison between far-UV/optical colour Magnitude Diagrams obtained with high-resolution *Hubble Space Telescope* data and suitable theoretical models for three Galactic Globular Clusters: M3, M13 and M79.

These systems represents a “classical” example of clusters in the intermediate metallicity regime that, even sharing similar metal content and age, show remarkably different Horizontal Branch morphologies. As a consequence, the observed differences in the colour distributions of Horizontal Branch stars cannot be interpreted in terms of either first (metallicity) or a second parameter such as age.

We investigate here the possible role of variations of initial Helium abundance (Y). Thanks to the use of a proper setup of far-UV filters, we are able to put strong constraints on the maximum Y (Y_{max}) values compatible with the data. We find differences $\Delta Y_{max} \sim 0.02 - 0.04$ between the clusters with M13 showing the largest value ($Y_{max} \sim 0.30$) and M3 the smallest ($Y_{max} \sim 0.27$). In general we observe that these values are correlated with the colour extensions of their Horizontal Branches and with the range of the observed Na-O anti-correlations.

Key words: Globular clusters: individual (M3, M13, M79); stars: evolution – Horizontal Branch; ultraviolet: stars

1 INTRODUCTION

Horizontal branch (HB) stars are the progeny of low-mass Red Giant Branch stars (RGB) burning helium in their cores and hydrogen in a shell around it (Hoyle & Schwarzschild 1955). As first noticed by Iben & Rood (1970), the different HB star colour distributions observed in old stellar systems, is the reflection of the amount of mass lost during the RGB phase.

The scientific community agrees from nearly fifty years about the fact that the principal parameter governing the shape of HBs in Galactic Globular Clusters (GGCs) is metallicity. The general rule is that metal-rich systems have red HBs, while in the metal-poor ones stars are distributed on average at higher effective temperatures (bluer colours). Several exceptions have come out during the last decades; remarkable cases the cases of NGC6388 and NGC6441 (Rich et al. 1997), which despite their metallicity ($[Fe/H] \sim -0.6$) show some of the bluest HBs known among GGCs (Busso et al. 2007; Dalessandro et al. 2008). Moreover several clusters, sharing similar metal content, reveal different HB morphologies, typical cases being the pairs NGC5927 - NGC6388 at

high metallicities ($[Fe/H] \sim -0.4$), M3 - M13 at intermediate metallicity regime ($[Fe/H] \sim -1.5$; Ferraro et al. 1997) and M15 - M92 at low metallicities ($[Fe/H] \sim -2.3$).

These noticeable exceptions have required the introduction of a second (Freeman & Norris 1981) and possibly a third parameter in order to explain the HB distributions in all GGCs. What we can call now the “*i-th parameter problem*” is still a hot topic, as stressed by several authors, we recall the reader to Catelan 2009 for a nice review (see also Dotter et al. 2010 and Gratton et al. 2010; hereafter D10 and G10 respectively).¹

An accurate knowledge of the physical parameters playing a role in shaping the HB is extremely important also for an appropriate interpretation of distant unresolved stellar populations. In fact it is well known that the HB morphology can have a strong impact on the integrated light of stellar populations, affecting colours and line indices (Lee et al. 2002;

¹ Moreover the increase of photometric capabilities has allowed to reveal tiny differences and features like gaps along the HB of some GGCs (see Ferraro et al 1998 for example), has complicated the interpretation.

Schiavon et al. 2004; Percival & Salaris 2011; Dalessandro et al. 2012).

Despite the huge efforts made to address this problem, its solution is not obvious and still different scenarios are proposed. One of the reasons that complicates the identification of the mechanisms – other than metallicity – at work in shaping the observed luminosity and effective temperature distribution of stars along the HB is that there are many possible culprits (mass-loss, age, helium abundance ...; see Rood 1973 for example) and some of them are not well constrained from theory.

Age has been identified as the natural global second parameter by many authors in the past years (Lee et al. 1987, 1988, 1990; Lee, Demarque & Zinn 1994; Sarajedini & King 1989). According to this interpretation older clusters tend to have bluer HBs, while younger ones should have on average redder HB morphologies. This scenario appeared in agreement with the picture for the Galaxy formation and its early evolution (Searle & Zinn 1978; Zinn 1985). By means of high resolution HST data for a large sample of GGCs, D10 found that the existence of outer halo GCs with anomalously red HBs fits well the scenario in which age is the second parameter. In fact, the behaviour of the 4-5 relatively younger clusters in their sample could be reproduced in term of correlation between age and HB morphology, while the bulk of the analyzed targets is peaked around old ages (see ages reported by Salaris & Weiss 2002, G10, D10) and doesn't show any obvious correlation. Also results by G10 agree on the fact that age is the second main parameter driving the HB morphology.

It is also worth noticing that most of these results are based on optical CMDs and HB morphology parameters (like the well known HBR from Lee et al. 1994), which tend to minimize the importance of blue tails. On the contrary using proper combinations of Ultra-Violet (UV) and optical filters has an important impact both in term of HB classification and comparison with theoretical models.

Still, age is not able to explain exhaustively the HB morphology. Detailed cluster to cluster comparisons have shown that there are systems with similar iron content and age, but remarkably different HB morphologies. A clear example is given by the three clusters M3 - M13 - M80, as shown by Ferraro et al. (1997, 1998) and at present there is hardly a scenario able to give a satisfactory explanation for their different morphologies.

As suggested by Buonanno et al. (1985) and Fusi Pecci et al. (1993), age might be one of many and probably the most important HB second-parameter, but not the only one. Buonanno et al. (1995) argued that it is not possible to reproduce the complex HB zoology with a single “global” parameter, but more likely we can explain it by thinking of a “global combination” of “non-global” quantities and phenomena related to the formation, chemical and dynamical evolution of each cluster.

The necessity of at least a third parameter transpires also from D10 and G10 analyses, in the form of either the luminosity cluster density or stellar density ($\log(\rho)$) – as already suggested by Fusi Pecci et al. (1993) – which might correlate with the hot extension of the HBs, or a variation of the initial helium abundance (Y), respectively.

Indeed D'Antona et al. (2005) and Dalessandro et al. (2011 – hereafter PaperI) have shown that for NGC2808 the main

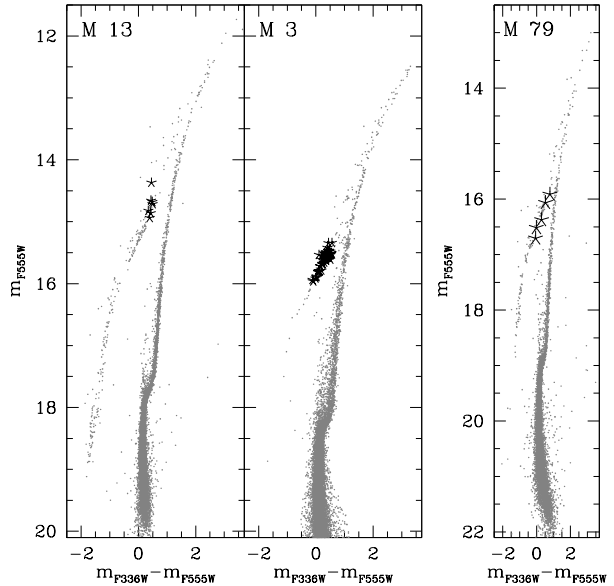


Figure 1. Optical CMDs of the three GGCs considered in our analysis.

parameter that determines the HB morphology is Y . In particular in PaperI we have been able to satisfactorily reproduce the cluster complex HB morphology by assuming three different sub-populations with He abundances compatible with what inferred from the multimodal Main Sequence (MS; Piotto et al. 2007) and spectroscopic analyses (Bragaglia et al. 2010; Pasquini et al. 2011). It is worth noticing however that only few clusters show evidences of multiple sub-populations with different He abundances as inferred from their MS or spectroscopic analyses (NGC2808, ω Centauri – Bedin et al. 2004, NGC6752 – Milone et al. 2010, NGC6397 – Milone et al. 2012; NGC1851 – Gratton et al. 2012)

In order to further investigate the “*i*-th parameter problem”, we selected a triplet of GGCs with similar metallicity ($[Fe/H] \sim -1.50$) and age, namely NGC5272 (M3), NGC6205 (M13) and NGC1904 (M79) as templates for a comparative analysis of their HBs. These targets are basically the same used by Ferraro et al. (1997, 1998), with the only exception of M80, which have been replaced by M79 since recent spectroscopic analyses (Carretta et al. 2009) show that it is slightly more metal-poor than the others. As shown by Ferraro et al. (1998), M13 has a very extended HB with two clear gaps (named G1 and G2 after their analysis); while, the HB of M3 covers a much narrower extension in effective temperature and shows only a mild indication for a gap at the same T_{eff} as G1 in M13. M79 represents an intermediate case between the two.

As already done for NGC2808 (Paper I) we will use a combination of optical and UV photometric images. Details about data reduction are presented in Section 2. In Section 3 we will focus on the long-standing debate about the age-differences between these clusters. Comparisons with theoretical models and cluster-to-cluster differences will be discussed in Section 4 and 5.

2 OBSERVATIONAL DATA SETS AND DATA REDUCTION

The data-set used in the present work consists of Hubble Space Telescope (HST) Wide Field Planetary Camera 2 (WFPC2) images. All targets have been observed in the $F555W$, $F336W$ and $F160BW$ bands, the only exception is M3 for which no $F160BW$ data are available. (see Table 1). Images and photometry obtained in other bands are also available for some of the clusters, however as shown in Rood et al. 2008 and Paper I the combination of $F555W$, $F336W$ and $F160BW$ seems to be the best filters setup to study both RHBs and stars lying at the very hot end of the HB. The photometric catalogues of M3 and M13 have been already partially presented by Ferraro et al. (1998), while the photometry of M79 has been already used by Lanzoni et al. (2007). Moreover Far-UV photometry of M79 and M13 has been presented by Rood et al. (2008) in order to describe in detail the advantages of using the combination of $F160BW$ and $F555W$ magnitudes for comparison with HB models.

In all cases the photometric analysis has been performed by using ROMAFOOT (Buonanno et al. 1983). The reduction strategy has been optimized to be particularly sensitive to hot stars, as already described by Ferraro et al. (2003). For the present analysis attention has been paid to the cross-identification of stars detected in the $F160BW$ images. Stars observed only in these bands have been force-fitted in the other bands (see Paper I).

The instrumental magnitudes have been calibrated to the VEGAMAG photometric system by using zero-points and the gain settings reported in Table 5.1 of the WFPC2 *data handbook Manual*². Magnitudes thus obtained have been also corrected for Charge Transfer Efficiency (CTE) effect by means of the prescriptions by Dolphin (2000) and updated equations listed in the dedicated page of Dolphin’s web site³.

The resulting colour Magnitude Diagrams (CMDs) for each cluster are shown in both the $(m_{F160BW}, m_{F160BW} - m_{F555W})$ and $(m_{F336W}, m_{F336W} - m_{F555W})$ planes in Figs 1 and 2.

Star lists have been reported to the absolute coordinate system by mean of proper roto-traslations. In particular, for each cluster the instrumental coordinates have been reported to the GSCII astrometric standard system by using a large number of primary and secondary standards in common, consisting typically of Wide Field ground-based data-sets, in the WFPC2 Fields of View (FOVs) (see Lanzoni et al. 2007 for details). At the end of the procedure, the typical error of the astrometric solution is $\sim 0.2''$.

2.1 RR Lyrae identification

The identification of variable stars lying along the HB is a crucial step to perform a suitable comparison between observations and theoretical models. This is particularly true in case of M3, that hosts tens of RR Lyrae stars.

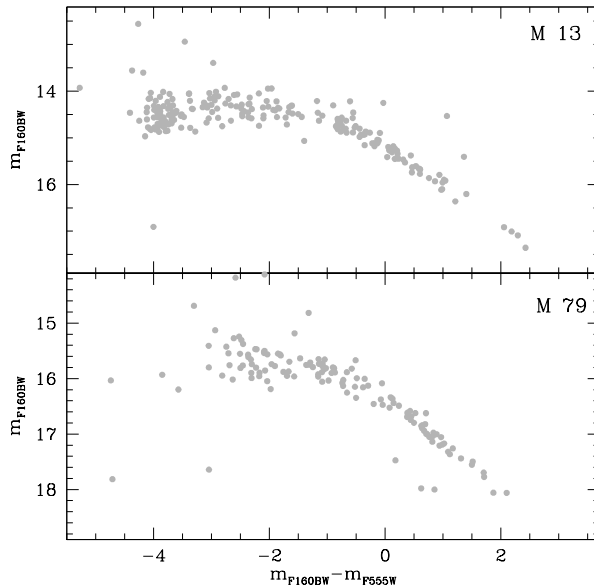


Figure 2. Far-UV CMDs of M13 and M79.

However, none of the data-sets used here is designed for variability search, both because of the short time baseline covered and number of images acquired. In our CMDs, variables are basically sampled at random phase. Thus we decided to use publicly available catalogues of variable stars in order to cross-identify them in our photometric catalogues, as already done in Paper I. We retrieved position, magnitude, and classification lists from the ‘‘Catalogue of Variable Stars in Galactic Globular Clusters (2011)’’⁴ (Clement et al. 2001). We refer to that paper for all details and references. We focused only on RR Lyrae stars, neglecting all the other different variable types. We first roto-traslated the catalogues of variables to our reference frames by using CataXcorr, a software developed at the Bologna Observatory (Montegriffo, private communication). We then looked for stars in common with our photometry. All the known RR Lyrae stars in our FOVs have been recovered in our catalogues. We found 59 RR Lyrae in M3, 7 in M13 and 5 in M79 (see Table 1). Their positions in the optical CMDs are shown in Figure 1.

3 METALLICITY AND RELATIVE AGES

An accurate determination of metallicities and ages is a crucial point for HB morphology studies and for the correct interpretation of comparative analyses.

The three GGCs in our sample have a similar iron content: according to the recent reassessment of the GC metallicity scale by Carretta et al (2009), metallicities are equal to $[\text{Fe}/\text{H}] = -1.50 \pm 0.05$, -1.58 ± 0.04 and -1.58 ± 0.02 for M3, M13 and M79, respectively. Consistent results were also found by Sneden et al. (2004) who obtained $[\text{Fe}/\text{H}] = -1.55 \pm 0.02$ and -1.57 ± 0.07 for M3 and M13

² <http://www.stsci.edu/documents/dhb/web/>

³ <http://purcell.as.arizona.edu/>

⁴ <http://www.astro.utoronto.ca/~cclement/read.html>

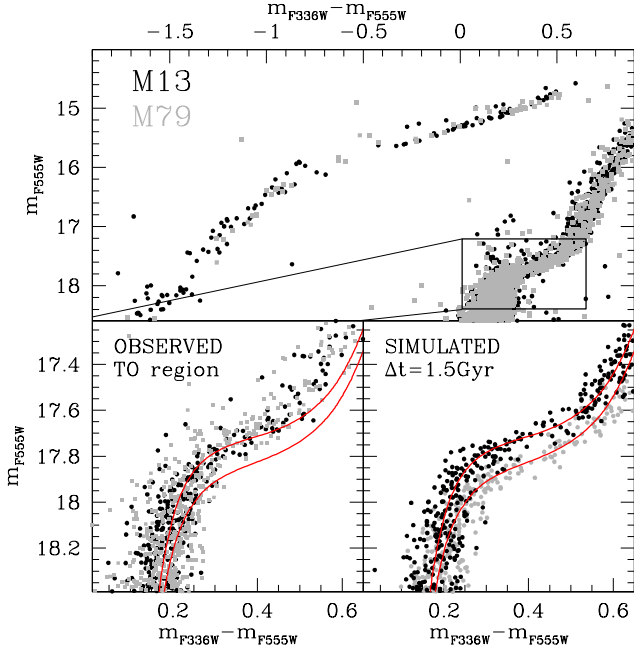


Figure 3. Upper panel. Optical CMD of M79 super-imposed to M13 after correcting for differences in distance modulus and reddening. Bottom panels. Zoomed view of the TO region. On the left, the observed CMDs are shown with two isochrones from the BaSTI database with $t = 12$ Gyr and $t = 13.5$ Gyr. The right panel shows synthetic CMDs obtained from the adopted isochrones and the appropriate photometric errors.

(for homogeneity we report only values obtained from the Lick Hamilton spectra). Only in the analysis by Cohen & Melendez (2005) M3 and M13 are slightly more metal-rich, i.e. $[\text{Fe}/\text{H}] = -1.39 \pm 0.02$ and $[\text{Fe}/\text{H}] = -1.50 \pm 0.01$. In addition in this case the observed metallicity difference ($\Delta[\text{Fe}/\text{H}] \sim 0.1$) is larger than the uncertainties.

On the contrary the determination of their ages is a more debated argument. In literature there is a quite general consensus that M3 and M79 are old and coeval GGCs. There is instead more uncertainty about the age of M13. Ferraro et al. (1997) put constraints on the possible difference in age between M13 and M3 by comparing their ridge mean lines obtained with the optical CMDs used in this work, and theoretical models by Dorman et al. (1996). The age difference resulted to be smaller than $\Delta t = 1 - 1.5$ Gyr. The same conclusions have been reached also by Johnson & Bolte (1998) and Rosenberg et al. (1999). According to the analysis by Grundahl et al. (1999) M13 may be younger than M3 by 0.7 ± 0.2 Gyr, while for Rey et al. (2001) it is older by about 2 Gyr.

Ages reported by other authors for the clusters of our analysis agree quite well within the error bars. Salaris & Weiss (2002) found a typical difference smaller than $\Delta t = 1$ Gyr independently of the metallicity scale used. Ages by D10 obtained using the isochrone-fitting method are basically identical; in fact $t = (12.5 \pm 0.5)$ Gyr and $t = (13.0 \pm 0.5)$ Gyr for M3 and M13 respectively, while M79 is not in their

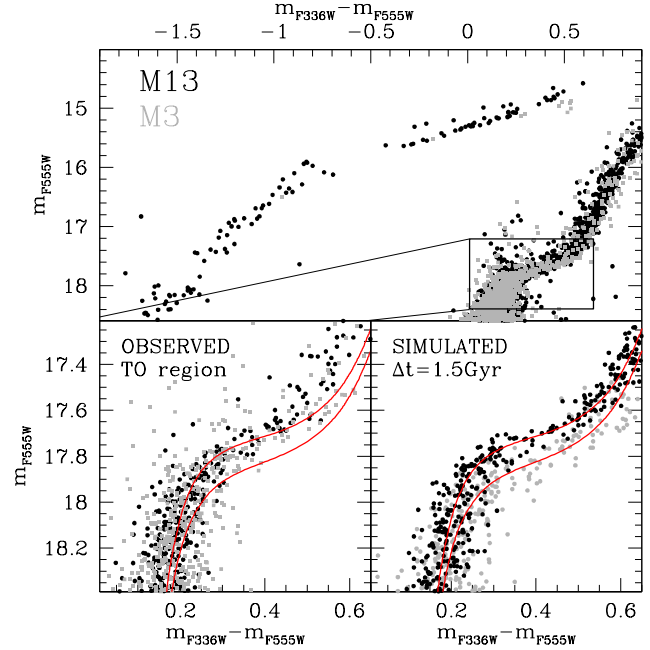


Figure 4. As in Fig. 3 but for M3 and M13.

sample. The same results were obtained by Marin-Franch et al. (2009). For G10 instead, M13 is older than M3 and M79 of about $\Delta t = 1.75$ Gyr.

It is worth noticing that even moderate differences of the average Y among these three clusters do not affect appreciably the results of the methods employed to determine their relative ages (see, e.g., Marin-Franch et al. 2010).

We investigated any possible age difference by comparing the $(m_{F555W}, m_{F336W} - m_{F555W})$ CMDs of the three clusters of our analysis.

We used M13 as reference and shifted M79 and M3 according to the difference of $E(B - V)$ values and distance moduli (see Sections 3.2, 3.3 and 3.4 for details about the values adopted). As apparent from the upper panels of Figure 3 and 4, once relative differences in reddening and distance are taken into account, the CMDs match well at the TO level and along the RGB, consistently with the fact that they have almost the same age and share a similar metallicity.

In the bottom panels we focus on their Turn Off (TO) region. Also from a close inspection, the CMDs have been found to nicely overlap at the TO and SGB region. This already rules out any significant age difference between M13, M3 and M79. However in order to perform a more accurate comparison, we also used two isochrones of proper metallicity and different age from the BaSTI database (Pietrinferni et al. 2006). In particular we used as reference the isochrone that best fits the observed CMD ($t = 12$ Gyr) and an additional one that is 1.5 Gyr older⁵. As apparent from the left bottom panels of Figures 3 and 4, the older isochrone does

⁵ Note that the aim of this analysis is not to obtain an estimate of the absolute age, but only to give constraints on relative ages

not match either the TO or the SGB.

Starting from these isochrones, and using the estimated photometric errors we build two synthetic populations of similar size to the observed ones for each comparison. With the typical uncertainties of our HST catalogues at the TO magnitude level, an age difference of 1.5 Gyr would be clearly visible and detectable. We then conclude that M13, M3 and M79 differ in age by less than 1 – 1.5 Gyr. This result is in agreement with estimates by several authors (Johnson & Bolte 1998; Rosenberg et al. 1999; Salaris and Weiss 2002; Marin-Franch et al. 2009; D10), while it is incompatible with the age differences proposed by G10. It is worth noticing that an age difference of about 1.5 – 2 Gyr would be compatible with the observed data only assuming extremely different He abundances ($\Delta Y \sim 0.1$) between these clusters.

4 THEORETICAL FRAMEWORK

We have shown that M3, M13 and M79 have similar metallicities and are coeval within typical uncertainties. Therefore in this case, the scenario proposed by G10 and D10, identifying the *second parameter* with age, is not applicable. We therefore investigate here the possible role of variations of Helium abundances in the framework of GCs having experienced multiple formation bursts (D’Ercole et al. 2008; Conroy & Spergel 2011; Valcarce & Catelan 2011) on a short timescale ($t \leq 100$ Myr) in environments enriched by material polluted by AGB stars (Ventura et al. 2002) or fast rotating stars (Decressin et al. 2007). As highlighted before, Helium has been proposed also by G10 to be the possible HB *third parameter*.

As in Paper I, we have compared our photometric data with a suitable set of BaSTI⁶ α -enhanced HB tracks (Pietrinferni et al. 2006). We have considered theoretical models for $[\text{Fe}/\text{H}] = -1.62$, which is the closest value available in the BaSTI database to the clusters spectroscopically determined $[\text{Fe}/\text{H}]$.

In our analysis we take advantage of all initial He-abundances available in the BaSTI database, i.e. $Y=0.246, 0.300, 0.350$ and 0.400 . Bolometric corrections and extinction effects have been calculated as in Paper I.

Recently, Gratton et al. (2011) have found spectroscopic evidence of a moderate Na-O anti-correlation in stars belonging to the HB of NGC2808, at T_{eff} below ~ 12000 , that marks the onset of radiative levitation effects (see discussion below). A similar result has been found for M 4 by Marino et al. (2011), the general trend being that the bluer HB stars are on average more Na-rich and O-poor. As a consequence of these empirical results, we verified by performing a number of tests (see Appendix A) how adequate is the use of ‘standard’ α -enhanced spectra to determine bolometric corrections in this temperature regime. We found that results obtained by using standard α -enhanced bolometric corrections, are unaffected by the presence of the observed CNONa anti-correlations.

Regarding the effect of radiative levitation, spectroscopic investigations by Behr (2003), Moehler et al. (2003),

Fabbian et al. (2005) have disclosed that - similar to the case of NGC2808 - in these three clusters HB stars hotter than ~ 12000 K display surface abundances of metal species like Fe, Cr and Ti around solar or higher, due to radiative levitation in the atmosphere. Also, the surface He abundances are depleted by a factor of ten or more as a consequence of gravitational settling. Following the approach used in Paper I, we mimic this effect using ‘standard’ α -enhanced HB stellar models by applying bolometric corrections appropriate for $[\text{Fe}/\text{H}]=0.0$ (and scaled-solar mixture) when T_{eff} is above 12000 K. This is of course a crude approximation, which we are forced to adopt because of the lack of extended grids of both HB stellar evolution and atmosphere models with a large range of chemical compositions, that include consistently the effect of radiative levitation. The underlying assumptions are that (i) the HB model evolutionary lifetimes, (ii) the evolution of T_{eff} and (iii) bolometric luminosity, and (iv) the structure of the corresponding model atmospheres are not affected by the radiative levitation, and that the relevant bolometric corrections are determined mainly by the enhanced metals. With these assumptions the effect of radiative levitation on bolometric corrections makes m_{F160BW} fainter by about 0.15 and m_{F336W} and m_{F555W} brighter by about 0.1 and 0.05 respectively. Paper I has shown how this approximation allowed us to recover the three different He-abundances inferred by the multimodal MS, along the blue HB of NGC2808. We are therefore confident that a similar procedure will be adequate to constrain the He distribution along the HB of these three clusters, that we are going to discuss separately in the following section.

4.1 The synthetic HB simulations

The theoretical analysis performed in this paper is based on synthetic HB calculations, performed as described in Paper I. The analysis of NGC2808 was simplified by the fact that the initial He content of the cluster subpopulations is somewhat ‘quantized’, as shown by the observed trimodal MS (Piotto et al. 2007). In case of M13, M3 and M79 there is no apparent ‘quantization’ of the MS, and we need to consider the possibility of a continuous distribution of Y along the HB.

We stress here that in these cases the modeling of the Y variations along the HB becomes more uncertain since calculations require more assumptions. Therefore the main goal of this work is not to attempt an exact description of the Y distribution, that would be affected by our assumptions, but to understand whether helium plays a role in shaping these very different HBs. UV filters are much better suited than optical ones to address this issue.

Our synthetic HB calculations require the specification of at least 4 parameters, plus the cluster age, that we assume to be equal to 12 Gyr (see Section 3). These four parameters are the minimum value of Y (Y_{min}), the range of He abundances (ΔY), the mean value of the mass lost along the RGB ΔM – that in first instance (and for simplicity) we assume to be the same for each Y – and the spread around this mean value ($\sigma(\Delta M)$). Throughout our analysis we will assume that Y varies according to either a uniform probability distribution, from Y_{min} to $Y_{\text{min}} + \Delta Y$, or a Gaussian one. In this latter case ΔY is the 1σ spread around a prescribed mean value. Also for the RGB total mass loss

⁶ Available at the following URL: <http://www.oa-teramo.inaf.it/BASTI>.

we will assume a Gaussian distribution around the mean value ΔM or a uniform distribution with minimum value equal to ΔM . The idea behind this type of simulations (see, e.g., Caloi & D’Antona 2005) is that the colour extension of the HB is driven mainly by the variation of Y rather than mass loss efficiency. A higher initial Y implies a lower mass at the tip of the RGB (for a fixed cluster age) hence, for a fixed value of ΔM , a smaller mass along the HB and a bluer colour (the He-core mass is affected by the variation of Y to a smaller extent). Our synthetic HB code first draws randomly a value of Y , and determines the initial mass of the star at the RGB tip (M_{TRGB}) from interpolation among the BaSTI isochrones of the prescribed age. The mass of the corresponding object evolving along the HB (M_{HB}) is then given by $M_{\text{HB}} = M_{\text{TRGB}} - \Delta M$ plus a Gaussian random perturbation $\sigma(\Delta M)$ (or a uniform probability between ΔM and $\Delta M + \sigma(\Delta M)$). The WFPC2 magnitudes of the synthetic star are then determined according to its position along the HB track with appropriate mass and Y – obtained by interpolation among the available set of HB tracks – after an evolutionary time t has been randomly extracted. We determined t assuming that stars reach the ZAHB at a constant rate. We employed a flat probability distribution ranging from zero to t_{HB} , where t_{HB} denotes the time spent from the ZAHB to the He-burning shell ignition along the early AGB. The value of t_{HB} is set by the mass with the longest lifetime (the lowest masses for a given Y and Z). This implies that for some synthetic object the randomly selected value of t will be longer than its t_{HB} or, in other words, that they have already evolved to the next evolutionary stages. Finally, the derived synthetic magnitudes are perturbed with a Gaussian 1σ error determined from the data reduction procedure.

We detail now the effects on these results of possible variations of age and chemical composition within the uncertainties described in Section 3. The mass distribution along the HB (as derived in our analysis) does not depend on the cluster age, but changing the cluster age changes the mass loss necessary to reproduce the HB mass distribution. An increase of age of 1 Gyr leads to a decrease of the total mass loss along the RGB by $\sim 0.02 M_{\odot}$ (because of the decreased evolving mass).

One can simulate the effect of a variation of $[\text{Fe}/\text{H}]$, $[\alpha/\text{Fe}]$ and/or their sum by considering that at these metallicities scaled solar and α -enhanced models (also for the HB) with the same total global metallicity $[\text{M}/\text{H}]$ are coincident (Salaris et al. 1993). We have therefore considered a change $\Delta[\text{M}/\text{H}] = +0.3$ dex that corresponds to changes of $[\text{Fe}/\text{H}]$ or $[\alpha/\text{Fe}]$ or $[\text{Fe}/\text{H}] + [\alpha/\text{Fe}]$. We have two effects here. The first one is on the derived mass distribution (at fixed Y) along the HB. For the redder part of the HB we use the $(m_{F336W}, m_{F336W} - m_{F555W})$ colour. At fixed colour in the horizontal part of the $(m_{F336W}, m_{F336W} - m_{F555W})$ CMD, an increase $\Delta[\text{M}/\text{H}] = 0.3$ decreases the derived value of M_{HB} by $\sim 0.04 M_{\odot}$. For the blue tails we use the $(m_{F160BW}, m_{F160BW} - m_{F555W})$ CMD. At fixed $(m_{F160BW} - m_{F555W})$ an increase $\Delta[\text{M}/\text{H}] = 0.3$ decreases the derived value of M_{HB} by $\sim 0.01 M_{\odot}$. This means that if a larger mass loss is needed to explain the blue HB stars (compared to the mass loss needed to explain the redder population), an increase of $[\text{M}/\text{H}]$ tends to reduce this mass loss difference. The second effect is on the RGB mass (hence

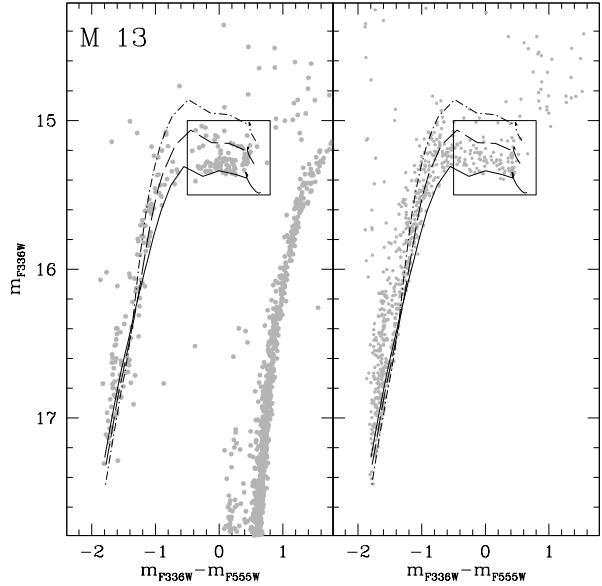


Figure 5. Observed (left panel) vs synthetic (right panel) $(m_{F336W}, m_{F336W} - m_{F555W})$ CMD of M13 HB. ZAHB sequences for $Y=0.246$ (solid line), 0.300 (dashed line) and 0.350 (dot-dashed line) are also displayed. The rectangular box marks the RHB region (see text for details).

on the absolute value of the RGB mass loss). An increase $\Delta[\text{M}/\text{H}] = 0.3$ causes an increase of M_{RGB} by $\sim 0.025 M_{\odot}$. The distribution of Y along the observed HBs is basically unaffected by the precise age and $[\text{M}/\text{H}]$, because it is based on the variation of magnitude (in m_{F336W} and m_{F160BW} , depending on the star colour) with Y , a differential property that is unaffected by the exact model metallicity and age.

5 COMPARISON BETWEEN THEORY AND OBSERVATIONS

In this section we will discuss separately the theoretical analysis of our three selected clusters. We stress again that allowing Y to vary within individual clusters, increases the number of free parameters needed to match the observed HB star distribution in the CMD. Leaving aside for a moment the open problem of the RGB mass loss, the distribution of Y among stars fed onto the HB will depend on the convolution of the unknown (at least for these three clusters) initial Y distribution among MS stars, with the Y -dependent evolutionary timescales along MS and RGB predicted by stellar models. As discussed before, in absence of constraints from the MS, we assumed here as a first order approximation either Gaussian or uniform probability distribution for Y among HB stars. As a consequence, the derived distribution of Y and mass range (at fixed Y) are most probably just a ‘reasonable’ approximation to the real ones. A much more solid result is the total range of Y covered by the stars in each individual cluster, because – thanks to our UV CMDs – this is strongly constrained by the observed stellar magnitudes m_{F160BW} (when available).

5.1 M13

Spectroscopic analyses of this cluster reveal a well developed Na-O anti-correlation (Snedden et al. 2004, Carretta et al. 2009), comparable to the case of NGC2808, but photometric analyses currently available do not show evidences for a multimodal MS. Here we analyze our HB photometry with – as stated before – the main aim of constraining the range of initial He values of the cluster stars. The use of the F160BW filter – not considered in the investigations by Caloi & D’Antona (2005) and D’Antona & Caloi (2008) – will set strong constraints on the maximum value of Y.

The first step of our analysis consists in defining the highest possible Y value necessary to fit the observed HB. To this purpose we calculated a synthetic HB with this preliminary set of parameters (uniform distributions for Y and Gaussian for M): $Y_{\min}=0.246$, $\Delta Y=0.104$, $\Delta M=0.21M_{\odot}$, $\sigma(\Delta M)=0.025M_{\odot}$. Even though this selection of parameters is not optimized for a perfect fit to the observed stellar distribution along the HB, it will suffice to put a first general constraint to the maximum possible range of initial Y. The number of stars in this simulation is higher than the observed sample, to reduce the effect of statistical number fluctuations on the synthetic HB.

The parameter ΔY has been arbitrarily fixed to reach the maximum He mass fraction $Y=0.35$. Once Y_{\min} is chosen, the mean RGB total mass loss ΔM is constrained by matching the red boundary of the observed HB (the subpopulation with the lowest Y has the largest HB mass at fixed age and ΔM). The value of $\sigma(\Delta M)$ then introduces a general dispersion in the relationship between HB colour and local He abundance. The smaller the value of this parameter, the narrower the range of Y in a given colour bin along the HB. We notice that a very small value of $\sigma(\Delta M)$ ($\sigma(\Delta M)=0.005$ for example), would produce a sloped HB (brighter towards bluer colours because of a very tight colour-Y relationship) in the $(m_{F336W}, m_{F336W} - m_{F555W})$ CMD at colour $(m_{F336W} - m_{F555W}) > -0.5$, instead of the observed roughly horizontal structure (see Figure 5).

As done in Paper I, we determined the cluster distance modulus by fitting the synthetic data to the observed Red HB (RHB) (defined here as the region of the HB contained in the square box plotted in Figure 5) in the $(m_{F336W}, m_{F336W} - m_{F555W})$ plane. Notice how the RHB is roughly horizontal in this CMD, and allows us to estimate straightforwardly the cluster distance by comparing the synthetic data to the observed number distribution of objects in m_{F336W} , assuming a reddening $E(B-V)=0.02$ (see for example Ferraro et al. 1999). A fit to both the lower envelope – defined as the faintest magnitude bin where the star counts are at least 2σ above zero – of the observed binned distribution in m_{F336W} , and the mean value of the m_{F336W} RHB magnitudes ($\langle m_{F336W} \rangle = 15.26$) provides $(m - M)_0 = 14.32 \pm 0.05^7$, in fair agreement within the uncertainties with Ferraro et al. (1999; $(m - M)_0 = 14.43$). The left and right panels of Figure 5 show the observed and simulated $(m_{F336W}, m_{F336W} - m_{F555W})$ CMD, respectively. We have also over-imposed three ZAHBs for $Y=0.246$ (solid line), 0.300 (long dashed line) and 0.350 (dot-dashed line). Figure 6 is equivalent to Figure 5, but for

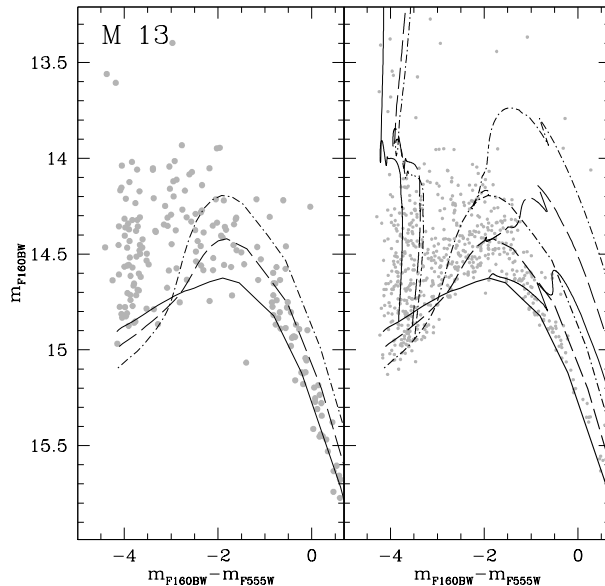


Figure 6. As in Figure 5 but for the $(m_{F160BW}, m_{F160BW} - m_{F555W})$ CMD (see text for details). In the right panel we also show two selected HB tracks corresponding to $M \sim 0.57M_{\odot}$ and $M \sim 0.50M_{\odot}$ for each ZAHB.

the $(m_{F160BW}, m_{F160BW} - m_{F555W})$ CMD. Whilst in the $(m_{F336W}, m_{F336W} - m_{F555W})$ CMD ZAHB sequences and synthetic stars with differing initial Y are largely degenerate along the bluest HB tail as a consequence of the huge increase of the bolometric correction in the optical filters, this same tail appears as a roughly horizontal sequence at $(m_{F160BW} - m_{F555W}) < -1.0$ in the $(m_{F160BW}, m_{F160BW} - m_{F555W})$ CMD. Theoretical ZAHB sequences display here different shapes at varying Y (see also Pietrinferni et al. 2006). It is clear from a comparison of the observed and synthetic HB that $Y=0.35$ for the bluest stars is too high. The lower envelope of the observed stellar distribution lies around the $Y=0.30$ ZAHB. This implies that the maximum Y (Y_{\max}) is ~ 0.30 .

As a conclusion, in the hypothesis that the colour extension of the HB is due to a range of initial Y values, $Y_{\min}=0.246$ at the red end of the observed HB implies $Y_{\max} \sim 0.30$ at the blue end, i.e. the initial He-abundance spans a range $\Delta Y \sim 0.05$. This constraint on Y_{\max} is very general; the critical discriminating factor is provided by the m_{F160BW} magnitude of the ZAHB at the blue end of the HB.

One can of course try a more accurate fit to the stellar distribution along the observed HB by comparing theoretical and observed histograms of star counts as a function of colour and magnitude. In this case a fine tuned calibration of the set of free parameters is necessary. In the assumption (for simplicity) of either uniform or Gaussian probability distributions for the mass loss and initial Y, one needs to split the simulation into three different sections, because no single continuous distribution of Y and mass allows to match the observed CMDs. As a general method – applied also to M3 and M79 –, for each choice of the free parameters we have produced 100 synthetic distributions, each of them with the

⁷ The error bar is equal to half the width of the adopted bin size

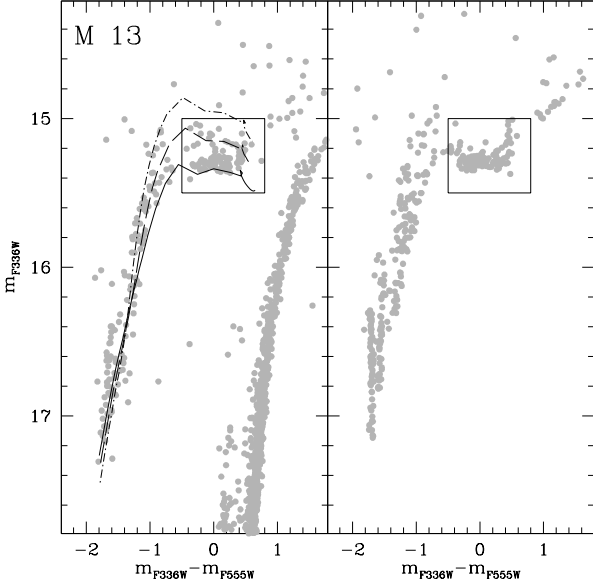


Figure 7. As in Figure 5 but for one realization of the best fit synthetic HB model discussed in the text.

same number of objects as in the observational sample. From this ensemble of simulations we have determined the mean value and associated error for each colour or magnitude bin used in their comparison with data.

The star counts along the RHB on the red side of the gap at $(m_{F336W} - m_{F555W}) \sim -0.5$ are best fit with $Y_{\min}=0.246$, $\Delta Y=0.01$ and uniform probability distribution for Y , $\Delta M=0.21M_{\odot}$, with a Gaussian spread $\sigma(\Delta M)=0.01M_{\odot}$. The resulting distance modulus is $(m - M)_0=14.30\pm 0.05$, quite similar to the value obtained from the simulation in Figure 5.

The second section of the simulation covers the region from the blue boundary of the gap to a colour $(m_{F160W} - m_{F555W}) \sim -3.0$ along the HB blue tail. In this case one needs a Gaussian distribution of Y , with mean value $\langle Y \rangle=0.285$ and 1σ spread $\Delta(Y)=0.012$, mass loss $\Delta M=0.235 M_{\odot}$ with a Gaussian spread $\sigma(\Delta M)=0.01M_{\odot}$. The last section of the simulation covers the extreme tail of the HB, that is best reproduced with $\langle Y \rangle=0.300$ with a Gaussian 1σ spread $\Delta(Y)=0.003$, and $\Delta M=0.266 M_{\odot}$ with a Gaussian spread $\sigma(\Delta M)=0.002M_{\odot}$. Figure 7 and Figure 8 display a comparison between the observed HB in the $(m_{F336W}, m_{F336W} - m_{F555W})$ and $(m_{F160BW}, m_{F160BW} - m_{F555W})$ CMDs, and one realization of the simulations with the parameter choice described before. From the parameters of this simulations, it is clear that a good match to the observed star counts can be obtained only by relaxing the assumption of constant ΔM for all initial He contents. In particular, it appears necessary to slightly increase on average ΔM when Y increases, as already highlighted in Paper I for the case of NGC2808. However it is important to note that, the maximum Y range is fully constrained independently of the assumptions on mass loss.

Note that the slight increase of ΔM with Y could be in principle due to an age variation at increasing Y . In this scenario the variation of ΔM corresponds to a variation of

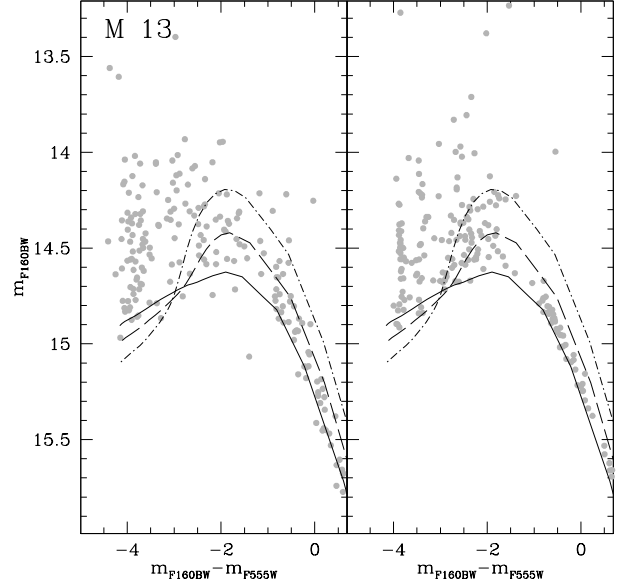


Figure 8. As in Figure 6 but for one realization of the best fit synthetic HB model discussed in the text.

M_{TRGB} with Y , keeping the total RGB mass loss unchanged. However, these mass differences imply an increase of age with increasing Y (lower mass evolving along the RGB) of the order of $\sim 4Gyr$ that is hard to justify. In fact such a large age difference would be detectable from the cluster TO and sub-giant branch regions, at odds with the empirical evidence (Figure 3 and Figure 4).

The mean He abundance along the HB of this simulation is $\langle Y \rangle=0.270$, with a 1σ spread $\sigma(Y)=0.02$. Notice that Salaris et al. (2004) determined for this cluster $Y=0.285\pm 0.024$ from the R-parameter, consistent with the results of the simulation.

We finally address the question of what happens if Y_{\min} in RHB stars is increased. As a test, we have first considered a constant $Y=0.280$ for the RHB – as proposed by Caloi & D’Antona (2005) and D’Antona & Caloi (2008) – and produced the corresponding synthetic population by tuning appropriately the value of the mass range along the RHB. The distance modulus derived from the m_{F336W} magnitudes of RHB stars is 0.14 mag larger than the case of our simulation with $Y_{\min}=0.246$. Given that the m_{F160BW} magnitude along the extreme blue tail of the observed HB increases with increasing Y (see Figure 6), this higher distance modulus would imply $Y \sim 0.25$ along the extreme HB ($(m_{F160BW} - m_{F555W}) < -3.5$), i.e. a value lower than along the RHB, a result justifiable only assuming a strong anti-correlation between mass loss and Y .

This test also implies that in principle, for a fine tuned Y_{\min} intermediate between 0.246 and 0.280, the whole HB of M13 can be also modeled – at least from the point of view of the magnitude levels in m_{F336W} and m_{F160BW} – employing a single value of Y . We find that when $Y_{\min} \sim 0.265$, the $(m_{F336W}, m_{F336W} - m_{F555W})$ and $(m_{F160BW}, m_{F160BW} - m_{F555W})$ observed CMDs and star counts can be reproduced with a constant He abundance, for a total mass spread of $\sim 0.14 M_{\odot}$. Even if we cannot discard this scenario on the

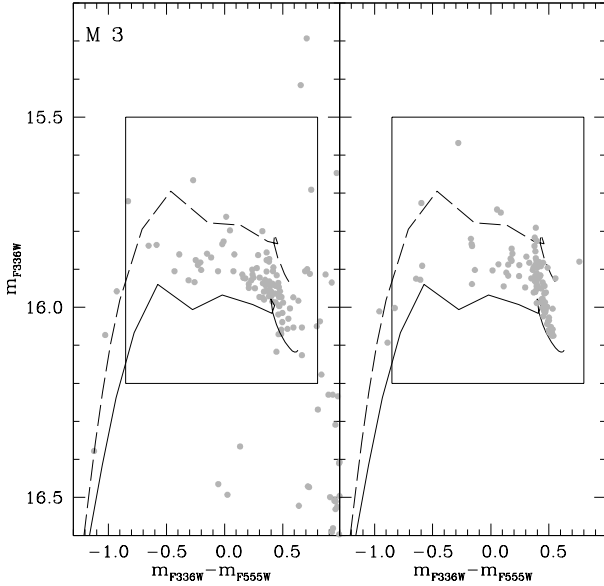


Figure 9. Observed (left panel) vs one realization of the best fit synthetic (right panel) ($m_{F336W}, m_{F336W} - m_{F555W}$) CMD of M3. The ZAHB sequences for $Y=0.246$ and $Y=0.300$ are also displayed. The rectangular box marks the region considered for the fit (see text for details).

basis of the HB analysis, we consider it very unlikely. In fact it would mean that M13 lost completely its first generation of standard He stars, while preserving most of the He-enriched population. This would be hardly compatible with results from N-body simulations (see for example Decressin, Baumgardt & Kroupa 2008).

5.2 M3

Spectroscopic analyses of M3 RGB stars reveal a Na-O anti-correlation that is reduced in extension compared to M13 (see, e.g., Sneden et al. 2004, Johnson et al. 2005 and references therein). Also in this case, the currently available photometric data do not show evidence of a multimodal MS. Also, as well known, the HB of M3 displays a much shorter colour extension compared to M13. Here we discuss its properties only in the ($m_{F336W}, m_{F336W} - m_{F555W}$) CMD, because no $F160BW$ images are available for this cluster. Given the way in which HB stars are distributed in all CMDs involving $F255W$, it doesn't give any additional information respect to the optical plane. Also given the relatively short extension of the HB of M3, we decided not to use the shorter wavelength $F255W$ filter.

We considered in our analysis all objects within the rectangular box in Figure 9. Our synthetic calculations show that all these stars have T_{eff} below the threshold for the onset of radiative levitation. There are three stars outside the box, that may be genuine HB objects, and appear spread along the bluest tail of the cluster HB, that is vertical also in this CMD. Given their extremely small number compared to the total sample of HB stars, and the fact that their location does not provide any further constraint on the cluster

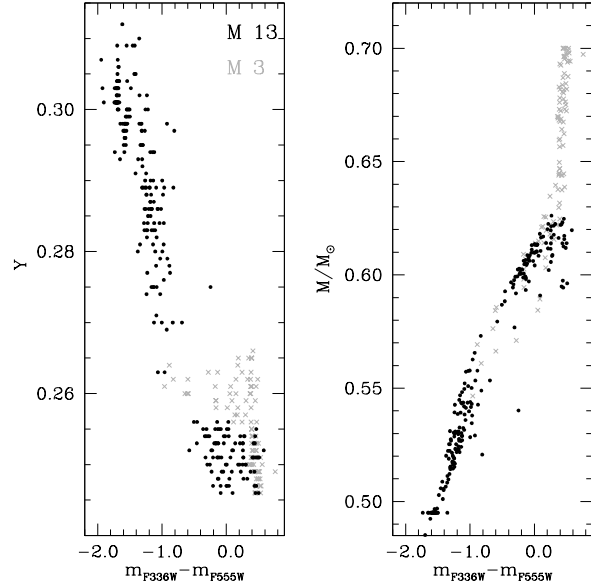


Figure 10. Mass and Y distribution as a function of the ($m_{F336W} - m_{F555W}$) colour along the HB of M3 (grey crosses) and M13 (black dots).

He distribution, we do not consider them in the theoretical analysis.

Following the same philosophy as for the case of M13, in the assumption of either uniform or Gaussian distributions for the mass loss and initial Y , observed star counts as a function of the m_{F336W} magnitude and ($m_{F336W} - m_{F555W}$) colour are best reproduced with $Y_{\text{min}}=0.246$, $\Delta Y=0.02$ and uniform probability distribution, a minimum RGB total mass loss $\Delta M=0.122M_{\odot}$ with a range (again uniform probability distribution) of values $\sigma(\Delta M)=9.0 \times (Y-0.246) M_{\odot}$, where Y is the actual initial He mass fraction of the synthetic star. It is obvious that this dependence of $\sigma(\Delta M)$ on Y – not imposed a priori but constrained by the fit to star counts as a function of magnitude and colour – implies an increase of the mass loss spread with increasing Y , that is required by the observed shape of the CMD in the ($m_{F336W}, m_{F336W} - m_{F555W}$) plane.

In fact as shown in Figure 9 the reddest part of the ZAHB describes a steeply sloped sequence, before turning horizontal at $m_{F336W} \sim 16.0$. To match the observed star counts we need to increase the mass loss spread with increasing Y . This is necessary to reproduce both the steep increase of m_{F336W} with decreasing colour when ($m_{F336W} - m_{F555W}$) is larger than ~ 0.2 – e.g., the lower He subpopulations have to cover a relatively small mass range – and the almost constant m_{F336W} when the colour ($m_{F336W} - m_{F555W}$) is bluer than this limit – e.g., the higher He subpopulations have to cover an increasingly larger mass range. The mean He abundance obtained from the synthetic HB is $\langle Y \rangle = 0.256$, with a 1σ spread $\sigma(Y)=0.006$, consistent with the value $Y=0.253 \pm 0.013$ obtained from the R-parameter by Cassisi et al. (2003). In the synthetic HB calculations we have disregarded all objects lying in the RRLyrae instability strip, whose red and blue edges have been fixed at, respectively, $\log T_{\text{eff}}=3.80$ and $\log T_{\text{eff}}=3.88$ (see, e.g., the discussion in

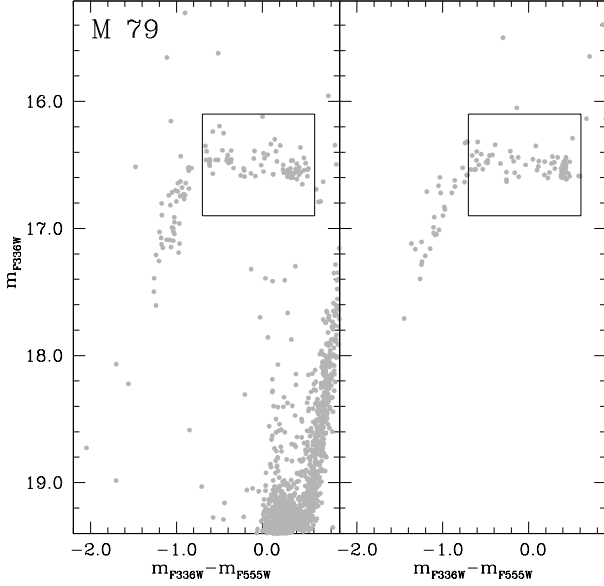


Figure 11. Observed (left panel) vs one realization of the best fit synthetic (right panel) $(m_{F336W}, m_{F336W} - m_{F555W})$ CMD of M79 HB. The box marks the region used for the estimate of the cluster distance (see text for details).

D’Antona & Caloi 2008), which define a very narrow colour width of $\Delta(m_{F336W} - m_{F555W}) < 0.05$ at fixed m_{F336W} approximately in the range $0.35 < (m_{F336W} - m_{F555W}) < 0.50$.

The distance modulus obtained as described in the case of M13 is $(m - M)_0 = 15.00 \pm 0.04$ with standard reddening value $E(B - V) = 0.01$ which is fully in agreement with previous estimates (Ferraro et al. 1999; Harris 1996 – catalogue version 2010). In this case the maximum value of Y ($Y_{\max} = 0.266$) is essentially constrained by the brightest limit of the stellar distribution at $(m_{F336W} - m_{F555W}) \sim 0.2$.

Figure 10 displays stellar mass and Y distributions as a function of the $(m_{F336W} - m_{F555W})$ colour in one representative synthetic realization of the cluster HB, compared to the corresponding best-fit composite simulation of M13. Not only the range of He values is obviously much larger in M13, but also the shape of the Y trend with colour is completely different in these two clusters. The mass distribution forms a very smooth continuous sequence, with the maximum and minimum masses along the HB distribution in M3 being appreciably larger than the corresponding values in M13.

A detailed comparison with recent results by Catelan et al (2009) and Caloi & D’Antona (2008) is reported in Appendix B.

5.3 M79

Spectroscopic analyses of M79 RGB stars disclose an extension of the Na-O anti-correlation that is intermediate between that of M13 and M3 (see Sneden et al. 2004, Carretta et al. 2010), and photometric analyses do not reveal evidences of a multimodal MS. Also the colour extension of its HB is intermediate between M13 and M3. Following the same approach as for M13 and M3, we find that observed

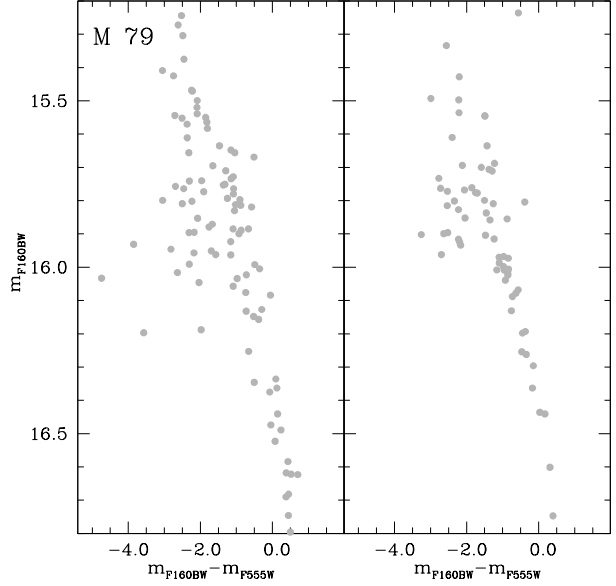


Figure 12. As in Figure 11 but for the $(m_{F160BW}, m_{F160BW} - m_{F555W})$ CMD (see text for details).

star counts as a function of magnitudes and colours are best reproduced with $Y_{\min} = 0.246$, $\Delta Y = 0.035$ and uniform probability distribution, a RGB total mass loss (at a given Y) ranging from $\Delta M = 0.11 M_{\odot}$ to $\Delta M = 0.27 M_{\odot}$, with a uniform probability distribution. One realization of the best fit simulation is displayed in Figures 11 and 12.

The distance modulus has been determined from the fit to the stars contained within the box displayed in Figure 11 (denoted here as RHB) as described for M13. Assuming $E(B - V) = 0.01$ (Harris 1996) we have obtained $(m - M)_0 = 15.64 \pm 0.05$, values well in agreement with both Ferraro et al. (1999) and Harris (1996). For the RHB stars we determine an average $\langle Y \rangle = 0.263$, with a 1σ spread $\sigma(Y) = 0.010$. The whole HB is characterized by $\langle Y \rangle = 0.265$, with a 1σ spread $\sigma(Y) = 0.010$. This means that the full range of Y values is already present in the RHB sample. In the reasonable assumption that the spread of initial Y scales with the extension of the Na-O anti-correlation, we should expect to find among RHB stars the full range of Na-O abundances observed along the RGB. A range of He abundances is necessary along the RHB to match the observed thickness in m_{F336W} , and the large range of ΔM (at fixed Y) is required to match the extended and almost horizontal structure of the RHB in the $(m_{F336W}, m_{F336W} - m_{F555W})$ CMD.

Figure 13 displays the mass and Y distribution as a function of the $(m_{F336W} - m_{F555W})$ colour in one representative synthetic realization of the cluster HB, compared to the M13 counterpart. The range of Y and the shape of the trend with colour are very different. The maximum mass of HB stars in M79 reaches higher values compared to M13, and the minimum HB mass is also higher than in M13.

Table 1. Filters adopted, number of observed HB and RR Lyrae stars and values of Y_{\max} and $\langle Y \rangle$ for the three clusters of our analysis.

| CLUSTER | FILTER | N_{HB} | N_{RRLyrae} | Y_{\max} | $\langle Y \rangle$ |
|---------|--------|-----------------|----------------------|------------|---------------------|
| M3 | F336W | 158 | 59 | 0.266 | 0.256 |
| | F555W | | | | |
| M13 | F160BW | 228 | 7 | 0.300 | 0.270 |
| | F336W | | | | |
| M79 | F160BW | 130 | 5 | 0.281 | 0.265 |
| | F336W | | | | |
| | F555W | | | | |

6 SUMMARY AND CONCLUSIONS

There is a general consensus that the first parameter shaping the globular cluster HB morphology is metallicity and the second one has been suggested by several authors (Lee et al. 2002; G10; D10) to be the age. While in general this picture may be surely adequate, however it is able to explain only few young clusters in the Galaxy, while it fails to reproduce a number of “classical” cases where an additional ingredient (sometime called third parameter) is required. The “third parameter” has been proposed to be the stellar density or luminosity density (Fusi Pecci et al. 1993; D10) or the initial helium abundance (G10).

In this framework we considered three GGCs with similar age and metallicity, M3, M13 and M79, with the aim of studying their HBs. According to G10, M3 is younger by ~ 2 Gyr than M13, however we find, in agreement with a number of authors (Salaris & Weiss 2002; Marin-Franch et al. 2009; D10), that these clusters differ in age by less than 1 Gyr.

This triplet is well known to have extremely different HBs, with M13 displaying by far the bluest morphology, and showing also evidence of at least 2 gaps at different effective temperatures, while M3 has been proposed over the years as a prototype of a “normal” HB.

As done in Paper I, we compared HST UV and optical CMDs with theoretical HB models, with the aim of understanding the impact (if any) of cluster-to-cluster Y variations on HB morphologies. At odds with the case of NGC2808, the three GCs analyzed in this work, do not show (so far) evidences of quantized MS, so our analysis has been performed without any a priori knowledge of the Y distribution. As explained in Section 4, this forced us to enlarge the parameters space: the quantities needed are the minimum value of Y (Y_{\min}) and its full range (ΔY), the mean value of the mass lost along the RGB ΔM and the dispersion around the mean value. As a consequence, it is hard in these cases to determine uniquely a full and detailed representation of the Y variations along the observed HBs. A more stringent and robust derivation involves instead the largest value of Y (Y_{\max}) that is clearly constrained by the distribution of stars in the (m_{F160BW} ; $m_{F160BW} - m_{F555W}$) CMDs. For the case of M3, given the shorter extension of its HB, the magnitudes m_{F336W} give already a strong constraint on Y_{\max} .

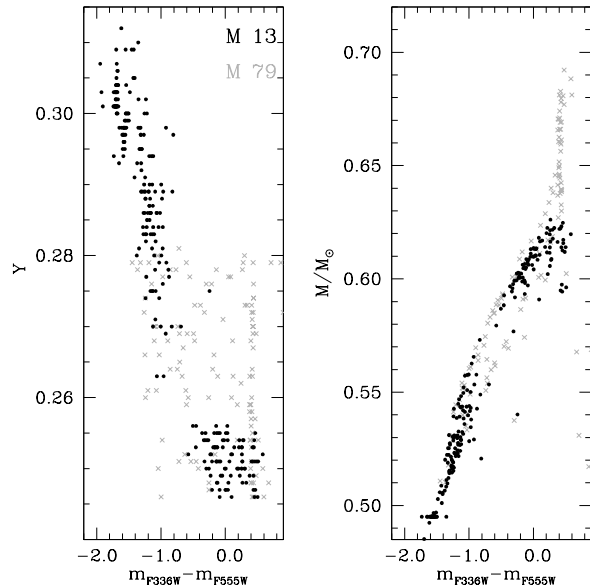


Figure 13. Mass and Y distribution as a function of the ($m_{F336W} - m_{F555W}$) colour along the HB of M79 (grey crosses) and M13 (black dots).

With these caveat in mind, we performed a detailed analysis by comparing observed CMDs with a large set of synthetic CMDs and ZAHBs from the BaSTI database (Pietrinferni et al. 2006). The effects of levitation for stars with $T_{\text{eff}} > 12000$ K and anti-correlations along the HBs (Marino et al. 2011; Gratton et al. 2011) have been considered.

We find differences $\Delta Y_{\max} \sim 0.02 - 0.04$ between these GGCs. In particular M13 displays the largest value ($Y_{\max} \sim 0.30$), M3 ($Y_{\max} \sim 0.27$) the smallest one, and M79 is an intermediate case with $Y_{\max} \sim 0.28$. These values are summarized in Table 1. They seem to qualitatively correlate with the differences in the temperature (colour) extensions of the cluster HBs. It is also interesting to note that our estimates of Y_{\max} for these three clusters nicely correlate with the observed range of light-element variations. In particular, M13 shows the most extreme Na-O anti-correlation (Snedden et al. 2004), with stars reaching $[\text{O}/\text{Fe}] = -1.1$ and $[\text{Na}/\text{Fe}] = 0.7$, while M3 the least extended one, $[\text{O}/\text{Fe}] = -0.2$ and $[\text{Na}/\text{Fe}] = 0.5$. This is in line with the strict correspondence between HB colours and Na-O abundances observed in NGC2808 by Gratton et al. (2011).

The comparison between M13 and M3 is particularly interesting, because of several previous analyses of their HB morphology and Y distribution. For example Catelan (2009) performed a detailed analysis comparing the mean masses of the HBs of these clusters with age differences proposed by different authors. By using several mass-loss recipes, he found that there is no way to reproduce the different HBs of M3 and M13 only in terms of age, but at least one additional ingredient should be invoked to account for the blue HB extension observed in M13. Our best-fit model for M13 requires to split the simulation in three steps, given that no single continuous distribution of Y and

mass loss allows to match the observed CMDs. Thus we divided the HB in three groups: 1) the RHB with a typical $Y_{\min} = 0.246$ and a mean mass lost = $\Delta M = 0.21M_{\odot}$, 2) stars with $-3 < (m_{F160BW} - m_{F555W}) < -1.5$ best reproduced with $\langle Y \rangle = 0.285$ and $\Delta M = 0.235M_{\odot}$ and 3) stars with $(m_{F160BW} - m_{F555W}) < -3$ which show a $\langle Y \rangle = 0.30$ and $\Delta M = 0.266M_{\odot}$. A fit with a population of stars with uniform $Y = 0.265$ cannot be ruled out on the basis of only the HB analysis, while a single population of stars with $Y = 0.28$, as proposed by Caloi & D’Antona (2005) and D’Antona & Caloi (2008), is incompatible with the distribution of stars in our UV CMD.

For M3 a single synthetic population with $Y_{\min} = 0.246$ and distributed according to a uniform probability distribution with $\Delta Y = 0.02$ is required. A total mass loss of $\Delta M = 0.122M_{\odot}$ and a linear increase as a function of Y , as constrained by the fit of star counts as a function of magnitude and colours, is needed. In the Appendix B we will discuss the Y distribution derived from our simulations in the context of the constraints posed by the analyses by Catelan et al. (2009) and D’Antona & Caloi (2008); it turns out that our estimate of $Y_{\max} = 0.266$ is robust.

As highlighted by G10, while M13 seems to behave as other relatively massive clusters, M3 appears to be peculiar and a more extended HB would have been expected in this case. The age difference proposed by G10 between these two clusters would justify at least in part the different HB morphology, in the framework in which age is the second parameter. Our results would instead lead to think that M3 and M13 experienced a different amount of enrichment of light elements. This would be compatible with the scenario proposed by G10 (see also Carretta et al. 2009) that invokes a delayed cooling flow in the case of M3. In particular the HB simulations and derived Y distributions would suggest that M13 is qualitatively similar to NGC2808, and that it likely experienced a similar star formation, while M3 (and M79) probably had a less complex formation history.

Analyses based on a suitable combination of UV to optical photometry – and when available observed RR Lyrae period distributions – and synthetic HB simulations can provide not only insights on the HB second parameter problem, but in general they can potentially give some clues on the first stages of GCs formation and chemical evolution.

We thank the referee Aaron Dotter for useful comments and suggestions that improved the presentation of this work. This research is part of the project COSMIC-LAB funded by the European Research Council (under contract ERC-2010-AdG-267675). SC acknowledges the financial support of the Ministero della Ricerca Scientifica e dell’Universita’ PRIN MIUR 2007: ‘Multiple stellar populations in globular clusters’, the Italian Theoretical Virtual Observatory Project and PRIN INAF 2011 ‘Formation and Early Evolution of Massive Star Clusters’

Appendix A

The effect of anti-correlations on bolometric corrections

We checked the impact of CNONa anti-correlations on the α -enhanced bolometric corrections by performing a number of tests. In particular, we have chosen three representative pairs of $(T_{\text{eff}}, \log(g))$ values along our theoretical α -enhanced ZAHB with $[\text{Fe}/\text{H}] = -1.62$, $Y = 0.246$, namely (5600 K, 2.40), (7000 K, 2.80), (10000 K, 3.50). For each of these pairs we have calculated a synthetic spectrum with the SYNTH code by R.L. Kurucz (Sbordone et al. 2005) in the wavelength range between 1200 and 7500 Å, including all the atomic and molecular lines available in the latest version of the Kurucz/Castelli linelist. The spectra were computed employing the LTE, plane-parallel model atmospheres calculated with the ATLAS12 code (Castelli 2005). ATLAS12 adopts the ‘opacity sampling’ method in the line opacity calculations, and allows to generate models for arbitrary chemical abundance mixtures. All the model atmospheres and synthetic integrated spectra were computed with $[\text{Fe}/\text{H}] = -1.62$ and $Y = 0.246$ and both the standard $[\alpha/\text{Fe}] = 0.4$ metal distribution used in the stellar evolution models, and the CNONa2 mixture by Sbordone et al. (2011). This latter mixture displays – compared to our reference α -enhanced mixture – enhancements of N and Na by 1.44 dex and 0.8 dex by mass, respectively, together with depletions of C and O by 0.6 dex and 0.8 dex, respectively, and unchanged CNO sum. This mixture is representative of extreme values of the CN and NaO anti-correlations observed in globular cluster stars (see Sbordone et al. 2011 for details). It is also very important to notice that low-mass stellar evolution models calculated for this mixture turn out to be identical to models calculated with the standard α -enhanced metal distribution.

From the synthetic spectra we have calculated bolometric corrections to the F160BW, F336W and F555W filters used in our analysis, for both metal mixtures. Only at $T_{\text{eff}} = 5600$ K there is a difference for the F336W filter (we did not consider the F160BW at this low temperature, because our photometry does not register cold HB stars in this passband) that amounts however to only 0.03 mag (CNONa2 mixture stars appearing fainter). Given the small value of this difference and the fact that such extreme values of the anti-correlations appear not to be reached at such low temperatures along the HB, the outcome of our analysis of NGC2808 and the results of this paper, based on standard α -enhanced bolometric corrections, are unaffected by the presence of the observed CNONa anti-correlations.

We have explicitly determined also the effect of He variations (at fixed metal content) on the bolometric corrections. We considered the point with (7000 K, 2.80) – i.e. around the blue edge of the RR Lyrae instability strip – and calculated spectra for our standard α -enhanced metal distribution, with $Y = 0.35$. Compared to the case with standard $Y = 0.246$, both F336W and F555W bolometric corrections are changed by less than 0.01 mag. The F160BW filter is affected at this level by less than 0.02 mag.

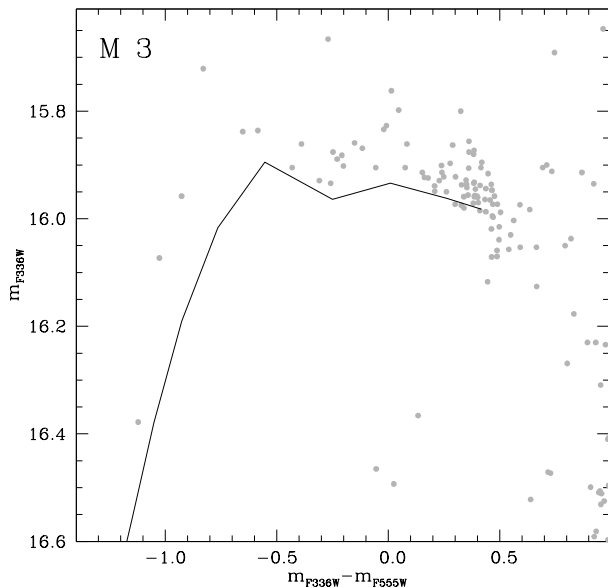


Figure 14. Comparison of M3 HB with a ZAHB sequence with $Y=0.256$, for $\log(T_{\text{eff}}) > 3.89$ (see text for details).

Appendix B

Comparison with previous studies on the HB morphology of M3.

We address here two issues that arise from a comparison with recent results from the literature about the HB morphology of M3. First of all, the range of Y derived from our simulations is about twice the value determined by Catalan et al. (2009) from a comparison of theoretical ZAHB magnitudes and gravities with both Strömrgren photometry, and spectroscopically measured surface gravities and T_{eff} . The size of the sample with spectroscopic gravities and T_{eff} estimates is relatively small, and within the corresponding error bars models with $Y \sim 0.27$ cannot be easily ruled out. More compelling seems to be the constraint from the Strömrgren CMDs. A fit of theoretical ZAHB models to the magnitude (y , b and v) of the lower envelope of the observed HB at both the red side of the instability strip and at the ‘knee’ of the stellar distribution beyond the blue edge of the strip, before the sparsely populated and not very extended blue vertical tail – where ZAHBs of different Y tend to become degenerate – discloses a range of Y at most equal to $\Delta Y \sim 0.01$, with Y increasing at the blue side of the strip. This disagreement with our results is however only apparent, for it can be very easily explained by recalling that to any given Y value corresponds it is associated a dispersion in colour along the HB (see Section 4.1). Figure 14 illustrates clearly this point by comparing a theoretical ZAHB for $Y=0.256$ and T_{eff} larger than the blue edge of the instability strip – shifted by our derived distance modulus and assumed reddening – to the observed data. Notice how for $(0.2 < (m_{F336W} - m_{F555W}) < 0.4)$, that corresponds to the region of the ‘knee’ in the Strömrgren CMDs, this ZAHB fits nicely the observed lower envelope of the CMD, even though the average Y in that colour range inferred by the best-fit

synthetic model, is 0.260. Given the existence of a range of HB masses at fixed Y , this colour interval is also populated by stars with Y as low as ~ 0.255 , that are on average the faintest objects and hence determine the observed lower envelope of the magnitude distribution.

The second issue is related to the cluster rich RR Lyrae population. The period distribution of fundamental RR Lyrae is strongly peaked, and in the recent literature attempts have been made to reproduce both the peaked period distribution and the HB colour extension. Castellani, Castellani, & Cassisi (2005) have shown that when keeping Y constant, a suitable bimodal mass distribution with two different mass dispersions is able to reproduce the observed features. On the other hand, D’Antona & Caloi (2008) assumed a range of Y and a very small mass dispersion for the mass loss along the RGB, and reproduced the observed HB colour extension and RR Lyrae periods by calibrating the Y distribution (instead of the HB mass distribution). It is interesting to notice that D’Antona & Caloi (2008) find from their simulations that 90% of HB stars are expected to have $Y \leq 0.265$, in agreement with our results, and only 10% of objects in their simulations reach Y values above our estimated maximum Y .

Here we have considered the synthetic objects in the best fit simulations that fall within the boundary of the instability strip (using the same T_{eff} boundaries employed by D’Antona & Caloi 2008) and were excluded from the comparison with the observed CMD. We have calculated their pulsational periods using the relationships by Di Criscienzo et al. (2004) and compared with the observed distribution (Corwin & Carney 2001). Our predicted period distribution does not reproduce the observed ones, which is probably not surprising given our ‘simple’ assumptions about the distribution of Y among stars fed onto the HB.

As a test, we have calculated additional synthetic HB models for M3, employing this time the *ad hoc* Y distribution⁸ proposed by D’Antona & Caloi (2008 – see their Figure 4) to reproduce both the observed period distribution in the instability strip and the $(B-V)$ colour distribution along the HB, while keeping the same mass loss for all HB stars. As in D’Antona & Caloi (2008) we employed a Gaussian mass distribution; our adopted mean mass loss is $\Delta M = 0.160 M_{\odot}$ with a small (as discussed in D’Antona & Caloi 2008) Gaussian spread $\sigma(\Delta M) = 0.002 M_{\odot}$, and employed the same reddening and distance modulus as in the previous simulations. These choices allow to reproduce well the narrow period distribution (both mean value of the logarithm of the periods and the 1σ dispersion) whereas a comparison of the the stellar distribution in the CMD at the blue side of the strip is less satisfactory. The left and right panels of Figure 15 show the observed and simulated $(m_{F336W}, m_{F336W} - m_{F555W})$ CMD. Notice how the observed shape of the CMD is reasonably reproduced as long as Y is below ~ 0.270 . For higher values of Y , synthetic stars tend to reach too bright magnitudes (while in the BV plane they tend to be located along the more vertical blue part of the HB, at/beyond the ‘knee’). This reinforces our estimate of the Y range as determined by our previous set of simulations – that is the main purpose of our analysis – and the need to increase the mass loss spread

⁸ Our minimum Y value is 0.246 instead of 0.240

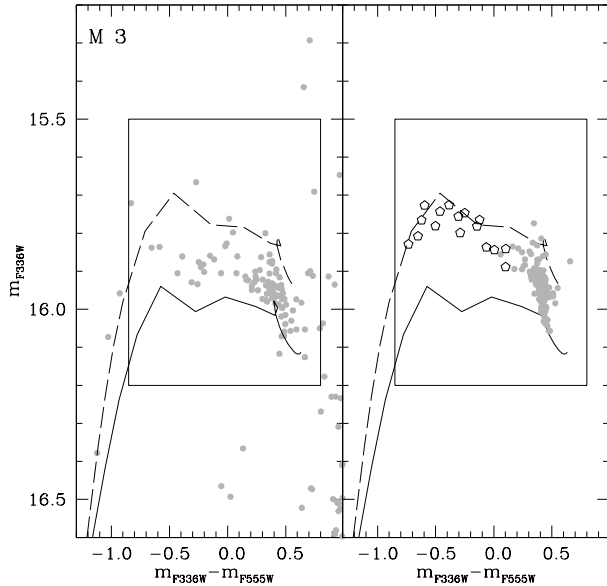


Figure 15. Observed (left panel) vs one realization of a synthetic (right panel) ($m_{F336W}, m_{F336W} - m_{F555W}$) CMD of M3 using the Y distribution proposed by D’Antona & Caloi (2008). Open symbols denote synthetic objects with $Y > 0.270$. The ZAHB sequences for $Y=0.246$ and $Y=0.300$ are also displayed. The rectangular box marks the region considered in the comparison (see text for details).

at the blue side of the instability strip – instead of Y – in order to match the CMD location of the bluer objects.

REFERENCES

- Bedin, L. R., Piotto, G., Anderson, J., et al. 2004, *ApJ*, 605, L125
- Behr, B. B. 2003, *ApJS*, 149, 67
- Bragaglia, A., Carretta, E., Gratton, R. G., et al. 2010, *ApJ*, 720, L41
- Buonanno, R., Buscema, G., Corsi, C. E., Ferraro, I., & Iannicola, G. 1983, *A&A*, 126, 278
- Buonanno, R., Corsi, C. E., & Fusi Pecci, F. 1985, *A&A*, 145, 97
- Busso, G., et al. 2007, *A&A*, 474, 105
- Caloi, V., & D’Antona, F. 2005, *A&A*, 435, 987
- Carretta, E., Bragaglia, A., Gratton, R., D’Orazi, V., & Lucatello, S. 2009, *A&A*, 508, 695
- Carretta, E., Bragaglia, A., Gratton, R. G., et al. 2010, *A&A*, 516, A55
- Castellani, M., Castellani, V., & Cassisi, S. 2005, *A&A*, 437, 1017
- Cassisi, S., Salaris, M., & Irwin, A. W. 2003, *ApJ*, 588, 862
- Castelli, F. 2005, *Memorie della Societa Astronomica Italiana Supplementi*, 8, 25
- Catelan, M. 2009, *APS&S*, 320, 261
- Catelan, M., Grundhal, F., Sweigart, A. V., Valcarce, A. A. R., & Cortés, C. 2009, *ApJ*, 695, L97
- Clement, C. M., Muzzin, A., Dufton, Q., et al. 2001, *AJ*, 122, 2587
- Cohen, J. G., & Melendez, J. 2005, *AJ*, 129, 1607
- Conroy, C., & Spergel, D. N. 2011, *ApJ*, 726, 36
- Corwin, T. M., & Carney, B. W. 2001, *AJ*, 122, 3183
- Dalessandro, E., Lanzoni, B., Ferraro, F. R., Rood, R. T., Milone, A., Piotto, G., & Valenti, E. 2008, *ApJ*, 677, 1069
- Dalessandro, E., Salaris, M., Ferraro, F. R., et al. 2011, *MNRAS*, 410, 694
- Dalessandro E., Schiavon R. P., Rood R. T., Ferraro F. R., Sohn S. T., Lanzoni B., O’Connell R. W., 2012, *AJ*, 144, 126
- D’Antona, F., & Caloi, V. 2008, *MNRAS*, 390, 693
- Decressin, T., Meynet, G., Charbonnel, C., Prantzos, N., & Ekström, S. 2007, *A&A*, 464, 1029
- Decressin, T., Baumgardt, H., & Kroupa, P. 2008, *A&A*, 492, 101
- D’Ercole, A., Vesperini, E., D’Antona, F., McMillan, S. L. W., & Recchi, S. 2008, *MNRAS*, 391, 825
- Di Criscienzo, M., Marconi, M., & Caputo, F. 2004, *ApJ*, 612, 1092
- Dolphin, A. E. 2000, *PASP*, 112, 1397
- Dotter, A., Sarajedini, A., Anderson, J., et al. 2010, *ApJ*, 708, 698
- Fabbian, D., Recio-Blanco, A., Gratton, R. G., & Piotto, G. 2005, *A&A*, 434, 235
- Ferraro, F. R., Paltrinieri, B., Fusi Pecci, F., et al. 1997, *ApJ*, 484, L145
- Ferraro, F. R., Paltrinieri, B., Pecci, F. F., Rood, R. T., & Dorman, B. 1998, *ApJ*, 500, 311
- Ferraro, F. R., Messineo, M., Fusi Pecci, F., et al. 1999, *AJ*, 118, 1738
- Ferraro, F. R., Sills, A., Rood, R. T., Paltrinieri, B., & Buonanno, R. 2003, *ApJ*, 588, 464
- Freeman, K. C., & Norris, J. 1981, *ARA&A*, 19, 319
- Fusi Pecci, F., Ferraro, F. R., Bellazzini, M., et al. 1993, *AJ*, 105, 1145
- Gratton, R. G., Carretta, E., Bragaglia, A., Lucatello, S., & D’Orazi, V. 2010, *A&A*, 517, A81
- Gratton, R. G., Lucatello, S., Carretta, E., Bragaglia, A., D’Orazi, V., & Momany, Y. A. 2011, *A&A*, 534, A123
- Grundahl, F., Catelan, M., Landsman, W. B., Stetson, P. B., & Andersen, M. I. 1999, *ApJ*, 524, 242
- Harris, W. E. 1996, *AJ*, 112, 1487
- Hoyle, F., & Schwarzschild, M. 1955, *ApJ*, 121, 776
- Johnson, J. A., & Bolte, M. 1998, *AJ*, 115, 693
- Johnson, C. I., Kraft, R. P., Pilachowski, C. A., et al. 2005, *PASP*,

- 117, 1308
- Iben, I., Jr., & Rood, R. T. 1970, ApJ, 161, 587
- Lanzoni, B., Dalessandro, E., Ferraro, F. R., Mocchi, P., Valenti, E., & Rood, R. T. 2007, ApJ, 668, L139
- Lee, Y.-W., Demarque, P., & Zinn, R. 1987, IAU Colloq. 95: Second Conference on Faint Blue Stars, 137
- Lee, Y.-W., Demarque, P., & Zinn, R. 1988, Calibration of Stellar ages, 149
- Lee, Y.-W., Demarque, P., & Zinn, R. 1990, ApJ, 350, 155
- Lee, Y.-W., Demarque, P., & Zinn, R. 1994, ApJ, 423, 248
- Lee, Y.-W., Lee, H.-C., Yoon, S.-J., Rey, S.-C., & Chaboyer, B. 2002, Extragalactic Star Clusters, 207, 110
- Marino, A. F., Villanova, S., Milone, A.P., Piotto, G., Lind, K., Geisler, D., Stetson, P.B. 2011, ApJ, 730, L16
- Marín-Franch, A., Aparicio, A., Piotto, G., et al. 2009, ApJ, 694, 1498
- Marín-Franch, A., Cassisi, S., Aparicio, A., & Pietrinferni, A. 2010, ApJ, 714, 1072
- Milone, A. P., Piotto, G., King, I. R., et al. 2010, ApJ, 709, 1183
- Milone, A. P., Marino, A. F., Piotto, G., et al. 2012, ApJ, 745, 27
- Moehler, S., Landsman, W. B., Sweigart, A. V., & Grundahl, F. 2003, A&A, 405, 135
- Pasquini, L., Mauas, P., Käufel, H. U., & Cacciari, C. 2011, A&A, 531, A35
- Percival S. M., Salaris M., 2011, MNRAS, 412, 2445
- Pietrinferni, A., Cassisi, S., Salaris, M., & Castelli, F. 2006, ApJ, 642, 797
- Piotto, G., Bedin, L. R., Anderson, J., King, I. R., Cassisi, S., Milone, A. P., Villanova, S., Pietrinferni, A., & Renzini, A. 2007, ApJ, 661, L53
- Rey, S.-C., Yoon, S.-J., Lee, Y.-W., Chaboyer, B., & Sarajedini, A. 2001, AJ, 122, 3219
- Rich, R. M., et al. 1997, ApJ, 484, L25
- Rood, R. T. 1973, ApJ, 184, 815
- Rood, R. T., Beccari, G., Lanzoni, B., Ferraro, F. R., Dalessandro, E., & Schiavon, R. P. 2008, Memorie della Societa Astronomica Italiana, 79, 383
- Rosenberg, A., Saviane, I., Piotto, G., & Aparicio, A. 1999, AJ, 118, 2306
- Salaris, M., Chieffi, A., & Straniero, O. 1993, ApJ, 414, 580
- Salaris, M., & Weiss, A. 2002, A&A, 388, 492
- Salaris, M., Riello, M., Cassisi, S., & Piotto, G. 2004, A&A, 420, 911
- Sbordone, L. 2005, Memorie della Societa Astronomica Italiana Supplementi, 8, 61
- Sbordone, L., Salaris, M., Weiss, A., & Cassisi, S. 2011, A&A, 534, A9
- Schiavon R. P., Rose J. A., Courteau S., MacArthur L. A., 2004, ApJ, 608, L33
- Searle, L., & Zinn, R. 1978, ApJ, 225, 357
- Snedden, C., Kraft, R. P., Guhathakurta, P., Peterson, R. C., & Fulbright, J. P. 2004, AJ, 127, 2162
- Valcarce A. A. R., Catelan M., 2011, A&A, 533, A120
- Ventura, P., D'Antona, F., & Mazzitelli, I. 2002, A&A, 393, 215
- Zinn, R. 1985, ApJ, 293, 424